Table 2 Parameters and RMSEs of Mooney–Rivlin (nine-constants) (11) and combined logarithmic and polynomial (22) models in representing combined cycle of compression and elongation experimental data of 6 porcine livers

	Mooney–Rivlin (nine-constants) (11)			Combined logarithmic and polynomial (22)	
	material parameters		RMSE, Pa	material parameters	RMSE, Pa
Liver 1	$C_1 = -0.19 \times 10^4$	$C_6 = 1.58 \times 10^4$	18.66	$C_1 = -1.67 \times 10^4$	95.35
	$C_2 = 0.22 \times 10^4$	$C_7 = -0.81 \times 10^4$		$C_2 = 0.571$	
	$C_3 = 0.29 \times 10^4$	$C_8 = 1.07 \times 10^4$		$C_3 = -4.50 \times 10^3$	
	$C_4 = -0.002 \times 10^4$	$C_9 = -0.61 \times 10^4$			
	$C_5 = -0.41 \times 10^4$				
Liver 2	$C_1 = -0.11 \times 10^4$	$C_6 = -3.95 \times 10^4$	24.88	$C_1 = -4.23 \times 10^4$	90.76
	$C_2 = 0.15 \times 10^4$	$C_7 = -3.41 \times 10^4$		$C_2 = 0.23$	
	$C_3 = 0.97 \times 10^4$	$C_8 = 6.65 \times 10^4$		$C_3 = -4.58 \times 10^3$	
	$C_4 = -0.49 \times 10^4$	$C_9 = -4.79 \times 10^4$			
	$C_5 = -0.52 \times 10^4$				
Liver 3	$C_1 = -0.23 \times 10^4$	$C_6 = 5.54 \times 10^4$	40.15	$C_1 = -6.38 \times 10^2$	104.69
	$C_2 = 0.26 \times 10^4$	$C_7 = -1.67 \times 10^4$		$C_2 = 1.62$	
	$C_3 = 0.63 \times 10^4$	$C_8 = -2.85 \times 10^3$		$C_3 = -4.14 \times 10^2$	
	$C_4 = 0.13 \times 10^4$	$C_9 = 1.36 \times 10^4$			
	$C_5 = -0.89 \times 10^4$				
Liver 4	$C_1 = -0.02 \times 10^4$	$C_6 = -0.92 \times 10^4$	20.22	$C_1 = -5.94 \times 10^3$	91.44
	$C_2 = 0.053 \times 10^4$	$C_7 = -0.02 \times 10^4$		$C_2 = 0.75$	
	$C_3 = 0.42 \times 10^4$	$C_8 = 2.54 \times 10^3$		$C_3 = -2.14 \times 10^3$	
	$C_4 = 0.11 \times 10^4$	$C_9 = -1.28 \times 10^4$			
	$C_5 = -0.46 \times 10^4$				
Liver 5	$C_1 = 0.11 \times 10^4$	$C_6 = 3.62 \times 10^4$	45.55	$C_1 = -8.55 \times 10^4$	105.83
	$C_2 = -0.07 \times 10^4$	$C_7 = -4.38 \times 10^4$		$C_2 = 0.57$	
	$C_3 = -0.50 \times 10^4$	$C_8 = -0.24 \times 10^3$		$C_3 = -9.63 \times 10^3$	
	$C_4 = 0.25 \times 10^4$	$C_9 = 1.09 \times 10^4$			
	$C_5 = 0.15 \times 10^4$				
Liver 6	$C_1 = -0.09 \times 10^4$	$C_6 = -0.25 \times 10^4$	35.37	$C_1 = -1.67 \times 10^4$	106.67
	$C_2 = 0.12 \times 10^4$	$C_7 = -0.65 \times 10^4$		$C_2 = 0.28$	
	$C_3 = 0.19 \times 10^4$	$C_8 = 2.11 \times 10^3$		$C_3 = -0.19 \times 10^4$	
	$C_4 = -0.09 \times 10^4$	$C_9 = -0.95 \times 10^4$			
	$C_5 = -0.15 \times 10^4$				

in material parameters. The polarity of the parameters did not change in the combined model. This demonstrates the suitability of our combined logarithmic and polynomial energy function as the model of choice for soft tissues in general, and liver tissue in particular. Note that experiments with porcine kidney and brain tissues are preliminary at five test samples each.

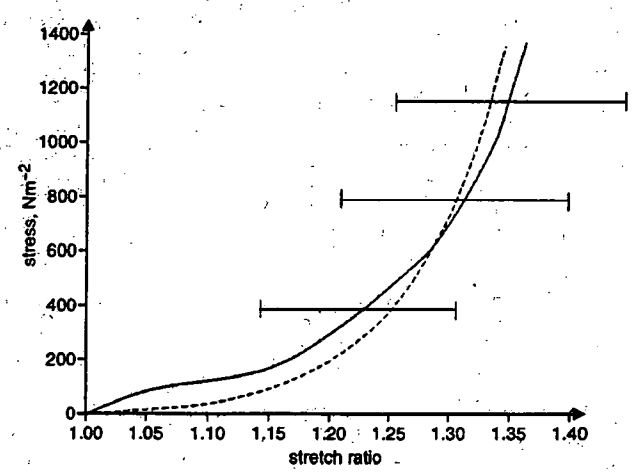

Fig. 9 *Validation of combined logarithmic and polynomial equation using experimental results from smaller samples. Sample diameter was 3 mm, with heights ranging from 5 mm to 6 mm. Number of samples tested was 4. Loading rate was 10 mm min^{-1}. Standard deviations from mean experimental values are indicated with horizontal bars. (—) Experiment; (– – –) Theoretical estimation*

5 Conclusions

In this paper, we have presented our model of the mechanical behaviour of liver based on conventional continuum mechanics, for surgical simulation applications. Our results obtained from *in vitro* uniaxial measurements showed that liver tissue deforms differently under compression and elongation. Thus, instead of relying on separate compression and elongation experiments to define the material properties of liver, we believe that a cycle with both compression and elongation should be used. To the best of our knowledge, this report is the first to express biomechanical properties of biological tissue based on complete cycles of compression and then elongation. The existing constitutive models did not fit this complete cycle of compression and elongation well.

We investigated and confirmed the hypothesis that a constitutive equation with both polynomial and logarithmic forms could best represent the stress–strain relationship of a complete cycle of compression and elongation. In fact, our combined logarithmic and polynomial equation provided an excellent fit over the entire stress–strain curve for separate compression and elongation. Besides demonstrating that our proposed combined logarithmic and polynomial model is the preferred model to represent the liver biomechanical properties, in a preliminary investigation, we found that this theoretical model could represent the stress–strain relationship of other soft tissues, such as porcine brain and kidney tissues.

The value of a model is in predicting actions based on theory of formulated quantitative mechanical properties and principles of physics. It is clear that our experimental and theoretical results agree under the conditions of our experimental design. Unfortunately, biological tissue properties change with disease, and this is the environment in which computer-aided surgery

is performed. We are aiming eventually to introduce parameters of pathology such as stiffness, from diseases such as cirrhosis, and compare cadaver results with experimental predictive data. Under normal conditions, the liver is heavily perfused with blood, both from hepatic arterial and portal venous sources. This perfusion imparts a certain degree of turgidity that is not present in unperfused samples. This will influence the deformation properties. The samples should be infused with solution resembling blood serum at a pressure consistent with that found in the liver. We are enhancing our current experimental measuring system to administrate the infusion process.

We agree with a reviewer that the biphasic model is a possible approach to the integration of the effect of blood pressure that will enhance the realism of surgical simulation of liver therapies. As was also hihlighted by the reviewer, the biphasic model poses a sufficient challenge, both theoretically and experimentally. The resultant biphasic model will possibly be highly complex and interactive, but near real-time computation is impossible with existing hardware. Hence, our work described here is possibly a more practical approach to surgical simulation. A practical application of our work includes simulation of liver deformation from RF needle insertion. In this application, the medical image of a patient's liver was classified into vessels and liver tissues. A finite element model of the liver was then created with elemental material properties defined according to the classified image. The defined material property and modelling of the liver tissues were related to the work described in this paper.

We assumed that liver is an isotropic material in this investigation. In another ongoing study, we have found that the correlation of coefficients obtained from the experimental data with those from theoretical predictions was generally better when transverse isotropy was assumed. This observation is in agreement with a study on constitutive modelling of lung tissue (VAWTER *et al.*, 1980). We have observed that liver tissue has some transverse anisotropy characteristics, and we are currently investigating these characteristics further. We also plan to carry out non-linear finite element simulations based on the tensor forms of our combined logarithmic and polynomial models (ONODERA *et al.*, 2001).

Acknowledgments—This research was supported in part by the Research for the Future Program (JSPS-RTFT99I00904). C. Chui is supported in part by the C&C Foreign Researcher Fund. He is also grateful to Professor J.H. Anderson from The Johns Hopkins University School of Medicine, Baltimore, USA, for many discussions on anatomy, physiology and surgery. The authors also wish to thank the reviewers for their valuable comments.

References

BOGEN, D. (1987): 'Strain-energy description of biological swelling. I Single fluid compartment models', *ASME J. Biomech. Eng.*, **109**, pp. 252–256

BRUYNS, C., and OTTENSMEYER, M. (2002): 'Measuring soft-tissue mechanical properties to support development of a physically based virtual animal model', in DOHI, T., and KIKINIS, R. (Eds): 'Lecture Notes in Computer Science 2488: Medical Image Computing and Computer-Assisted Intervention'. MICCAI 2002, pp. 283–289

CARTER, F. J., FRANK, T. G., DAVIES, P. J., MCLEAN, D., and CUSCHIERI, A. (2001): 'Biomechanical testing of intra-abdominal soft tissue', *Med. Image Anal.*, **5**, pp. 231–236

DAVIES, P. J., CARTER, F. J., and CUSCHIERI, A. (2002): 'Mathematical modelling for keyhole surgery simulation: a biomechanical model for spleen tissue', *IMA J. Appl. Math.*, **67**, pp. 41–67

DAVIES, P. J., CARTER, F. J., ROXBURGH, D. G., and CUSCHIERI, A. (1999): 'Mathematical modelling for keyhole surgery simulations: spleen capsule as an elastic membrane', *J. Theor. Med.*, **1**, pp. 247–262

DEMIRAY, H. (1972): 'A note of the elasticity of soft biological tissues', *J. Biomech.*, **5**, pp. 309–311

FARSHAD, M., BARBEZAT, M., SCHMIDLIN, F., BIDAUT, L., NIEDERER, P., and GRABER, P. (1998): 'Material characterization and mathematical modeling of the pig kidney in relation with biomechanical analysis of renal trauma'. Proc. North American Congress on Biomechanics, Waterloo, Ontario, Canada

FUNG, Y. (1967): 'Elasticity of soft tissues in simple elongation', *American J. Physiology*, **213**, pp. 1532–1544

FUNG, Y. (1993): 'Biomechanics—mechanical properties of living tissues', second edn, (Springer, New York, 1993)

FUNG, Y., LIU, S., and ZHOU, J. (1993): 'Remodeling of the constitutive equation while a blood vessel remodels itself under stress', *ASME J. Biomech. Eng.*, **115**, pp. 453–459

HAWKES, D. J., EWARDS, P. J., BARRATT, D., BLACKALL, J. M., PENNEY, G. P., and TANNER, C. (2003): 'Measuring and modeling soft tissue deformation for image guided interventions', in AYACHE, N. and DELINGETTE, H. (Eds): 'Lecture notes in computer science 2673: surgical simulation and soft tissue modeling', pp. 1–14

HAYASHI, K. (1993): 'Experimental approaches on measuring the mechanical properties and constitutive laws of arterial walls', *ASME J. Biomech. Eng.*, **115**, pp. 481–487

HISADA, T., and NOGUCHI, H. (1995): 'Principle and application of non linear finite element methods (in Japanese)', (Maruzen, Tokyo, Japan, 1995)

KYRIACOU, S. K., SCHWAB, C., and HUMPHREY, J. D. (1996): 'Finite element analysis of nonlinear orthotropic hyperelastic membranes', *Comput. Mech.*, **18**, pp. 269–278

MELVIN, J. W., STALNAKER, R. L., and ROBERTS, V. L. (1973): 'Impact injury mechanisms in abdominal organs', *SAE Trans.*, **730968**, pp. 115–126

MILLER, K. (2000): 'Constitutive modelling of abdominal organs', *J. Biomec.*, **33**, pp. 367–373

MILLER, K., and CHINZEI, K. (1997): 'Constitutive modelling of brain tissue: experiment and theory', *J. Biomech.*, **30**, pp. 1115–1121

MOONEY, M. (1940): 'A theory of large elastic deformation', *J. Appl. Phy.*, **11**, pp. 582–592

MUTHUPILLAI, R., LOMAS, D. J., ROSSMAN, P. J., Greenleaf J. F., MANDUCA, A., and EHMAN, R. L. (1995): 'Magnetic resonance elastography by direct visualization of propagating acoustic strain waves', *Science*, **269**, pp. 1854–1857

ONODERA, K., CHEN, X., and HISADA, T. (2001): 'Identification of biomechanical material properties of soft tissues (in Japanese)'. Proc. Japan Computational Engineering Society Ann. Conf. 2001, Tokyo, Japan

PATHAK, A. P., SILVER-THORN M. B., THIERFELDER, C. A., and PRIETO, T. E. (1998): 'A rate-controlled indentor for *in vivo* analysis of residual limb tissues', *IEEE Trans. Rehabil. Eng.*, **6**, pp. 12–20

SAKUMA, I., NISHIMURA, Y., CHUI, C., KOBAYASHI, E., INADA, H, CHEN, X., and HISADA, T. (2003): '*In vitro* measurement of mechanical properties of liver tissue under compression and elongation using a new test piece holding method with surgical glue', In AYACHE, N., and DELINGETTE, H. (Eds): 'Lecture notes in computer science 2673: surgical simulation and soft tissue modeling', pp. 284–292

SCHMIDLIN, F. R., THOMASON, M., OLLER, D., MEREDITH, W., MOYLAN, J., CLANCY, T., CUNNINGHAM, P., and BAKER, C. (1996): 'Force transmission and stress distribution in a computer simulated model of the kidney: an analysis of the injury mechanisms in renal trauma', *J. Trauma*, **40**, pp. 791–796

TAKAMIZAWA, K., and HAYASHI, K. (1987): 'Strain energy density function and uniform strain hypothesis for arterial mechanics', *J. Biomech.*, **20**, pp. 7–17

TANAKA, T., and FUNG, Y. (1974): 'Elastic and inelastic properties of the canine aorta and their variation along the aortic tree', *J. Biomech.*, **7**, pp. 357–370

VAWTER, D. L., FUNG, Y. C., and WEST, J. B. (1980): 'Constitutive equation of lung tissue elasticity', *ASME J. Biomech. Eng.*, **101**, pp. 38–45

VERONDA, D. R., and WESTMANN, R. A. (1970): 'Mechanical characterizations of ski-finite deformations', *J. Biomech.*, **3**, pp. 111–124

VOSSOUGHI, J. (1995): 'Constitutive modelling of biological materials', in BRONZINO, J. D. (Ed.): 'The biomedical engineering handbook' (CRC Press, 1995), pp. 263–272

XIE, J., ZHOU, J., and FUNG, Y. (1995): 'Bending of blood vessel wall: stress–strain laws of the intima-media and adventitial layers', *ASME J. Biomech. Eng.*, **117**, pp. 136–145
YAMADA, H. (1970): 'Strength of biological materials' (Williams & Wilkins, Baltimore, USA, 1970)
ZOBITZ, M. E., LUO, Z., and AN, K. (2001): 'Determination of the compressive material properties of the supraspinatus tendon', *ASME J. Biomech. Eng.*, **123**, pp. 47–51

Authors' biographies

CHEEKONG CHUI has contributed to over 50 scientific articles in journals and conferences, and is the inventor/co-inventor of 1 US patent and 5 pending patents, mainly in computer-aided surgery. In the Biomedical Precision Engineering Lab at The University of Tokyo, Japan, he focuses on multi-level constitutive modelling of liver tissue for emerging surgical procedures.

ETSUKO KOBAYASHI received her PhD in precision machinery engineering from The University of Tokyo, Japan in 2000. She is currently an assistant professor with the Institute of Environmental Studies, Graduate School of Frontier Sciences, The University of Tokyo. Her research interests are medical robotics and computer-assisted intervention.

XIAN CHEN is an associate professor at The University of Tokyo, Japan. He has been working on computational biomechanics since 1999. His current research interests include multi-physic phenomena of soft tissues, and contact problems in diarthrodial joints using nonlinear finite element method.

TOSHIAKI HISADA received his PhD in mechanical engineering from The University of Tokyo, Japan, in 1979. He is currently a professor, and is heading the Computational Biomechanics Lab at the Institute of Environmental Studies, Graduate School of Frontier Sciences, The University of Tokyo.

ICHIRO SAKUMA received the BS, MS, and PhD degrees in precision machinery engineering from The University of Tokyo, Tokyo, Japan, in 1982, 1984, and 1989, respectively. He was a research associate in The Department of Precision Machinery Engineering at The University of Tokyo from 1985 to 1987. He was a Research Instructor at Baylor College of Medicine, Houston, Texas, USA from 1990–1991. He was an associate Professor at The Department of Applied Electronic Engineering, Tokyo Denki University, Saitama, Japan, from 1992 to 1998. He was an Associate Professor at the Department of Precision Engineering in the Graduate School of Engineering, as well as at the Institute of Environmental Studies at the Graduate School of Frontier Sciences, at The University of Tokyo, from 1998 to 2001. He is currently a professor at the Institute of Environmental Studies at The University of Tokyo. His research interests are in bio-medical instrumentation, simulation of biomedical phenomena, computer-assisted intervention, and surgical robotics.

5-Aminolevulinic Acid 誘導による蛍光画像を用いた術中脳腫瘍同定

○清水 一秀[a], 小林 英津子[a], 丸山 隆志[b], 村垣 善浩[c], 伊関 洋[b,c], 佐久間 一郎[a]

[a]東京大学大学院新領域創成科学研究科, [b]東京女子医科大学脳神経外科, [c]東京女子医科大学大学院先端生命医科学研究所先端工学外科分野

Intraoperative Detection of Brain Tumor by Image Acquisition and Processing based on 5-Aminolevulinic Acid-Induced Fluorescence

K. Shimizu[a], E. Kobayashi[a], T. Maruyama[b], Y. Muragaki[c], H. Iseki[b,c], I. Sakuma[a]

[a] *Graduate School of Frontier Science, The University of Tokyo, Tokyo, Japan*

[b] *Department of Neurosurgery, Neurological Institute, Tokyo Women's Medical University, Tokyo, Japan*

[c] *Faculty of Advanced Techno-Surgery (FATS), Institute of Advanced Biomedical Engineering and Science, Graduate School of Medicine, Tokyo Women's Medical University, Tokyo, Japan*

Abstract: An image acquisition and processing method for assisting intra-operative detection of brain tumor and its boundaries using 5-Aminolevulinic Acid(5-ALA), a tumor-marker with fluorescence, is presented in this paper. When 5-ALA was administered to a living body it turns into a fluorescent substance called ProtoporphyrinIX(PpIX) only in pathologic lesion.. PpIX is excited by receiving blue light and emits red fluorescence by which we can know the existence of tumors. The fluorescence image was acquired by a high sensitive CCD camera equipped with an optical filter to eliminate reflected blue light. The image was automatically binarized with a statistic method and its edge was superimposed onto the original image to show the profile of fluorescent area. To perform an animal experiment for evaluation of the system, excessive amount of 5-ALA was administered to a pig. Although automatic detection of the boundary may contain some errors, display of multiple edge detection results under different threshold levels helps surgeon to identify the boundary.

Key words: Aminolevulinic acid, 5-ALA, ProtoporphyrinIX, Photo dynamic diagnosis, Brain tumor, CCD camera, Automatic binarization,

1. 緒言

悪性脳腫瘍の摘出手術においては，腫瘍の浸潤性により周辺組織との境界部分が不明瞭である点が問題となる．その判断は術者の経験･能力に委ねられるが，一方で神経組織は再生されないので過度の切除は脳機能を損なってしまう．腫瘍の除去率と患者の予後には密接な関係があるので，脳腫瘍の除去手術においては必要十分な領域のみの選択的な治療が理想である．そこで，腫瘍選択性をもつ物質として，血液の生合成過程での副産物である 5-Aminolevulinic Acid (5-ALA) を用いた術中腫瘍同定を行う．5-ALA は術前に患者に投与されると腫瘍細胞のみにおいて蛍光物質に変化するため，励起光を照射することで発生する蛍光により術中に治療対象部位を確認することができる[1]．これにより，腫瘍の取り残しを防ぎ，同時に過度の侵襲を避ける事を目的とする．本研究では術中に腫瘍の検索を行う部位において蛍光を発生させてその画像を取得し画像処理によって蛍光発生部位を術者に提示するシステムを構築した．

2．システム構成

2．0 前提

5-ALA 誘導蛍光物質(ProtoporphyrinIX: PpIX)の生体内における吸収波長ピークは 405[nm]，発光波長ピークは 635[nm]である[1]．

2．1 蛍光計測装置

励起光(半導体レーザ:406[nm]，18[mW], Digital Stream co., Tokyo, Japan)を直接照射することで蛍光を発生させる．反射光を除去しつつ蛍光のみを輝度として捉えるため 635±5[nm](FWHM) のバンドパスフィルタを備えた CCD カメラ(JK-TU53H/IK-TU51CU, Toshiba co., Tokyo, Japan)で画像を取得する．蛍光は微弱であるためカメラによりフレーム蓄光を行う．マクロレンズとして Micro Nikkor 105mm F2.8 (Nikon co., Tokyo, Japan)を用いる．画像は画像処理ボード IP7000(Hitachi co., Tokyo, Japan)を通して 512*480 [pixel]の YUV形式でPCに取り込む．システムの概要を Fig.1 に示す．

2．2 蛍光画像解析ソフトウェア

画像の二値化とエッジ抽出を行い，元画像に重ね合わせて表示するソフトウェアを開発した．二値化の

閾値は，Y 画像のヒストグラムに対して自動閾値選定を行うことで得た[2]．即ち，ヒストグラムを輝度値で二つのクラスに分けた際に両クラスのクラス間分散とクラス内分散の比が最大となるような閾値を求める．暗視下で励起光を照射しフィルタを通して得た蛍光画像から輪郭を抽出し，明視下での画像に重ね合わせる事で蛍光領域を提示する．

3. 実験

臨床での使用を想定し，動物実験を行った．ランドレース種のブタに 20[mg/kg]の 5-ALA を投与し 5 時間後に開頭して画像の取得を行った．ブタ脳は病的ではなく正常であるが，過剰量の投与により脳表全域に蛍光を呈するので生理条件下での実験が可能である．画像中で蛍光領域を限定するため観察用の 10[mm]角の穴を開けた板を脳表に設置し，その上から励起光であるレーザを円形に集光させて約 59[μW/mm²]として照射した．カメラは脳表垂直な向きにに設置しており視野幅は約 20[mm]とした．明視下での画像を取得後カメラにフィルタを装着し消灯してレーザを照射しながら蛍光画像を再取得した．蛍光画像は 30 フレーム蓄光（露光時間 1[s]）で撮影した．蛍光画像を Fig.2(a)に，エッジ抽出画像と明視下画像を重ね合わせた結果を Fig.2(b)に示す．また，蛍光の特性を確認するために，分光光度計(BTC111E, B&W Tek Inc. DE, USA）を用いて励起光を照射した際の脳表面の蛍光スペクトルを取得した(Fig.3)．

4. 考察

計測用の孔の中において，わずか 1[s]の蓄光により計測に十分な強度の蛍光画像を得ることが出来た．また，Fig.2(b)より，蛍光強度の強い部分が描出されており，明視下画像で位置を確認できることが分かる．画像右側上部において蛍光が弱く輪郭も侵食されているのは計測孔によって局面上の脳表に影が出来てしまったためである．Fig.3 のスペクトルは明確な 5-ALA 誘導蛍光の波形を示している．530[nm]付近に自家蛍光と見られる小さいピークが確認できるが，バンドパスフィルタの使用により蛍光のみを適切に選択できていると考えられる．しかし，正確な輪郭の決定は基準が曖昧である為に難しい．むしろ，閾値を連続的に変化させて蛍光の強度分布を表示するなど，柔軟性を持った輪郭選定アルゴリズムを検討する必要がある．尚，本方法はすでに臨床使用が始まっている内分泌外科領域での 5-ALA の応用[3]においても有用であると考えられ，導入を検討している．

文献

1) Walter Stummer , Intraoperative Detection of Malignant Gliomas by 5-Aminolevulinic Acid-induced Porphyrin Fluorescence , Neurosurgery, 42, (3), 518-526, 1998
2) 大津展之，判別および最小 2 乗基準に基づく自動しきい値選定法，電子通信学会論文誌，VoLJ-63D，349-356，1980
3) 清水一雄，5-Aminolevulinic acid(5-ALA)の応用－内分泌頸部外科手術に有用かつ簡便な術中副甲状腺の新同定法－，内分泌外科，21，(3)，2004

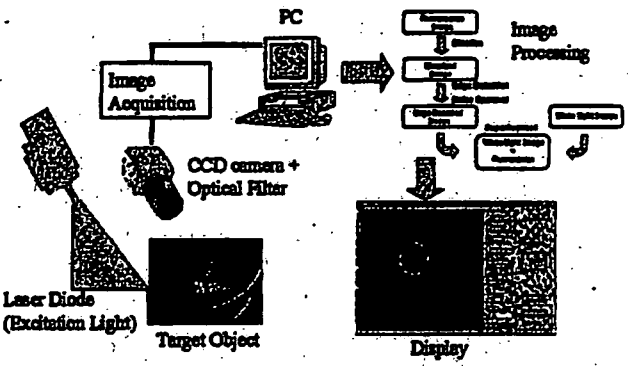

Fig.1 Sytem overview: consisting of a laser diode as excitation light, a CCD camera with an optical filter and a PC for image processing and display

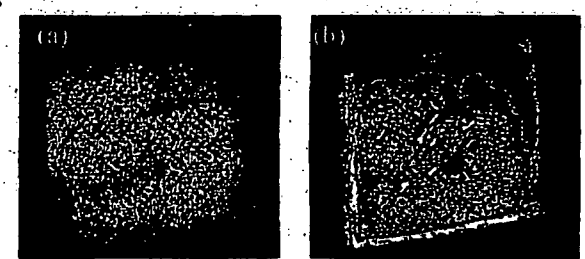

Fig.2 (a) Fluorescence image observed through an optical filter. (b) The original image under white light superimposed with the extracted edge (white line).

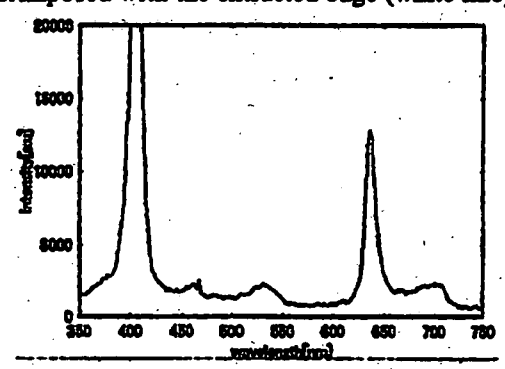

Fig.3 Spectrum from the surface of the fluorescent brain

04(XIV)-111 肝臓力学特性の実験的検討と構成式の導出

○佐久間一郎, 朱志光, 小林英津子, 陳献, 久田俊明
東京大学大学院新領域創成科学研究科環境学専攻

Experimental study on mechanical properties of liver and its constitutive equation

I. Sakuma, C. Chui, E. Kobayashi, X. Chen, T. Hisada
Institute of Environmental Studies, Graduate School of Frontier Sciences, The University of Tokyo, Tokyo, Japan

Abstract: Uniaxial stress-strain data were obtained from in vitro experiments on 20 porcine livers for compressions, elongations and cycle of compression and then elongation. There were about 70 cylindrical samples, with diameter 7mm and varying height (4-11mm). The combined compression and elongation test provide a uniform framework for both compression and elongation for application such as computer-aided surgical simulation and model based control of interventional devices. It enables zero stress state of the experimental liver sample to be precisely determined. A new equation that combined both logarithmic and polynomial strain energy forms was proposed in modeling these experimental data. The assumption of incompressibility was justified from a preliminary Poisson's ratio measurements for elongation and compression, respectively. This equation provided a good fit for the observed mechanical properties of liver during compression-elongation cycles and for separate compression or elongations. In comparison with existing strain energy functions, this combined model was the better constitutive equation.
Key words: Liver tissue, Compression and tensile test, Non-liniar elasticity, Mechanical properties, Computer aided surgery

1. はじめに

肝臓の力学特性を知ることは，コンピュータ外科における手術シミュレーションやモデルベースの治療機器制御システムの開発には重要である。

本研究の最終的な目的は変形する臓器である肝臓を対象とした手術シミュレーションシステムを構築するために求められる技術を開発することであり，肝臓の機械的特性の計測とそのモデリング技術，患者の医用画像に基づく患者臓器のモデリング技術，そしてこれらに基づいた手術機器と組織の相互作用や，組織の違いをも考慮した物理モデリング技術を開発することである。そのための基礎検討として，ブタ肝臓試験片に対する引張圧縮試験を実施し，実験結果をもとに，ブタ肝臓組織の構成式を導出した。

2. 肝臓試験片引張り圧縮試験 [1)]

肝臓の機械的特性の実験的検討では，20個のブタ肝臓から得られた70片の直径7mm高さ4－11mmの円筒状試験片に対して短軸引張圧縮試験を行った。応力ひずみ関係は非線形であった。引張圧縮を同一の試験片に加え実験を行うことによりコンピュータ外科への応用で重要となる応力0付近の特性も検討可能とした。

3. 構成式の導出と検証 [2)]

材料の非線形特性を表現する構成式を，ひずみエネルギー関数 W により表現した。変形のない状態での物体点 $\mathbf{X}$ が変形後 $\mathbf{x}$ に移動したとすると，変形勾配は

$$\mathbf{F}=\left(\frac{\partial \mathbf{x}}{\partial \mathbf{X}}\right)^{T} \qquad (1)$$

と与えられ，右 Cauchy-Green テンソル $\mathbf{C}$，テンソルの不変量は次のように与えられる。

$$\mathbf{C}=\mathbf{F}^{T}\mathbf{F} \qquad (2)$$

$$I=trace(\mathbf{C})=C_{ii},\quad II=trace(\mathbf{C}^{2})=C_{ij}C_{ji}$$

$$III=trace(\mathbf{C}^{3})=C_{ij}C_{jk}C_{ki} \qquad (2).$$

ひずみ不変量は.

$$I_1=I,\quad I_2=\frac{1}{2}(I^2-II)$$

$$I_3=\frac{1}{6}(I^3-3I\cdot II+2III)=\det(\mathbf{C}). \qquad (3)$$

で与えられる。このひずみ不変量の関数として肝臓のひずみエネルギーが $W(I_1,I_2,I_3)$ として表現できるものとする。なお肝臓を等方性材料と仮定した。

λ_1 を F の固有値とすると I_1 は λ_1 の関数となる。肝臓は圧縮引張時のポアソン比の計測結果よりほぼ非圧縮性とみなせた。非圧縮性を仮定し伸び率 $\lambda = \lambda_3$ と置くと $\lambda_1 = \lambda_2 = \frac{1}{\sqrt{\lambda_3}}$ となり，短軸引張圧縮状態での不変量 I_1, I_2, I_3 はそれぞれ

$$I_1 = \lambda^2 + 2/\lambda,\ I_2 = 2\lambda + 1/\lambda^2,\ I_3 = 1 \quad (4)$$

となる。

変形前の円筒状肝臓試験片の断面積を A_0 とすると，試料に加わる力を F とすれば公称応力は

$$T = \frac{F}{A_0} \quad (5)$$

で表され，試料の元の長さを L_0 とすると，試料の変位量は

$$\Delta L = L_0(\lambda - 1) \quad (6)$$

で表される。これらの値は実験値として得ることができる。一方ひずみエネルギー関数 W と T の関係は

$$T = \frac{2}{\lambda}\frac{\partial W}{\partial I_1}\left(\lambda^2 - \frac{1}{\lambda}\right) + \frac{2}{\lambda}\frac{\partial W}{\partial I_2}\left(\lambda - \frac{1}{\lambda^2}\right) \quad (7)$$

で与えられる。従ってひずみエネルギー関数形を仮定して推定される T と，実験結果から得られた T を比較することで肝臓試験片の変形挙動をよりよく表現する W を求めることができる。

検討の結果3つのパラメタ C_1, C_2, C_3 で表現する

$$W = \frac{-C_1}{2}\ln(1 - C_2(I_1 - 3)) + \left(\frac{C_3}{2} - \frac{C_1 C_2}{2}\right)(I_1 - 3) \quad (8)$$

という対数関数と多項式によりひずみエネルギーを表現する構成式を提案した。ひずみの大小により対数関数の寄与と多項式関数の寄与が入れ替わる。本ひずみエネルギー関数は圧縮引張の全区間にわたり肝臓試験片の非線形的な機械特性を Fig.1 に示すように表現することが可能であった。従来報告された. Mooney Rivlin モデルは9つのパラメタを持ち，提案した構成式より実験結果をよりよく再現できるが，提案した構成式が3つのパラメタのみで変形特性を記述できることから，計算効率の観点では優れている。また異なる実験結果を記述する場合に Mooney Rivlin モデルではパラメタの符号が変わることが見られ，有限要素解析の安定性に関して問題となるものと考えられたが，提案した構成式ではそのようなことはなかった。さらに検証として提案した構成式を圧子を肝臓組織に押し込むインデンテーション試験の解析に応用し，予測が可能であることを確認した。

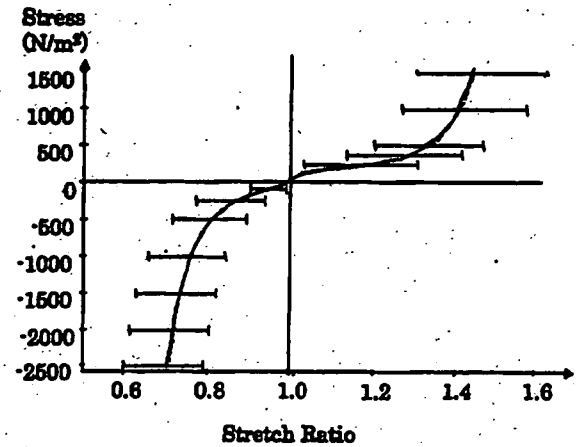

Fig. 1 Stress (T)–stretch (λ) graphs from uniaxial combined compression and elongation measurements with porcine liver tissue. There were 65 samples from 18 livers. The diameter and height of the cylindrical samples were 7 mm and 4-7 mm respectively. Loading rate was 10 mm/min. Solid and dash lines denote the mean and median values of the experiments respectively. Standard deviations from the mean values are indicated with horizontal bars.

まとめ

ブタ肝臓試験片に対する引張圧縮試験の結果を解析し，変形挙動を記述する対数関数と多項式によりひずみエネルギーを表現する構成式を提案した。本構成式は肝臓試験片の非線形的な機械特性を再現可能であった。

本研究の一部は，日本学術振興会未来開拓学術推進事業(99I00904),厚生労働省科学研究費補助身体機能解析・補助・代替機器開発研究事業(H15-ﾌｨｼﾞ-002)による。

文献

1) Sakuma, I. et al: Lecture Notes in Computer Science 2673: Surgical Simulation and Soft Tissue Modeling (In Ayache, N. and Delingette, H. ed.), pp 284–292, 2003.
2) Chui, C et al: Medical & Biological Engineering & Computing, in press

Development of a Compact Automatic Focusing System for a Neurosurgical Laser Instrument

M. Noguchi[1], E. Aoki[1], E. Kobayashi[1], S. Omori[2/3], Y. Muragaki[3], H. Iseki[3], I. Sakuma[1]

[1]Graduate School of Frontier Sciences, The University of Tokyo
[2]Terumo Corporation
[3]Faculty of Advanced Techno-surgery, Institute of Biomedical Engineering and Science, Graduate School of Medicine, Tokyo Women's Medical University

Abstract - **In neurosurgery such as the treatment of glioma, it is important to remove the tumor precisely and accurately, which can be achieved with a micro laser with a wavelength of 2.8 μm. It is necessary, however, to maintain a constant distance from the brain surface. In this research, we developed a compact automatic focusing system for the brain surface. We proposed the focusing method to appropriately control the luminance threshold in the image processing. We confirmed that this method works effectively on biomedical tissue. In the future, we will carry out a combination test with the micro laser system and achieve a precise operation system for brain tumors.**

Keywords – **Nerosurgery, laser, focusing, threshold, image processing.**

I. Introduction

In current neurosurgical practice, surgeons can remove most of a tumor with an accuracy of a few millimeters by using a combination of conventional surgical instruments, such as an electric cautery, and a computer-aided navigation system. Nevertheless, residual tumor may induce recurrence and it is necessary to remove as much of the tumor as possible while keeping the normal tissue intact. However, it is difficult to know the exact boundary between tumor and normal tissue, and excessive ablation of the normal brain tissue will damage its function.

For treatment of residual tumor, or tumors that cannot be treated by surgical intervention, pharmacotherapy or radiotherapy is applied. These methods are effective; however, there are problems such as side effects. Therefore, more precise surgical treatment than with conventional surgical instruments is desired.

To solve those problems, we have proposed a novel approach to therapy using 5-aminolevulinic acid (5-ALA) and a micro-laser ablation system, with the boundary between the tumor and the normal tissue distinguished by the 5-ALA fluorescence in the tumor [1], [2] and with accurate ablation of the tumor with the micro laser [3], [4]. The wavelength of the micro laser is 2.8 μm. Light with this wavelength is mostly absorbed by water, and therefore this laser is effective only on the surface of brain tissue, enabling precise ablation at the boundary between tumor and normal tissue. However, the focal depth of this laser is 1 mm, so the ablation depends on displacement from the focal point (Fig. 1). Therefore, a robotic automatic focusing system is necessary for the micro-laser ablation system. By the combination of the robotic positioning system and precise laser ablation, more accurate and precise operation is realized. In this research, we have developed an automatic focusing system for the microlaser ablation system, so as to achieve accurate operation in neurosurgery.

II. Method

A. Desired Specifications

We set the following requirements for the automatic focusing system.

1) Measurement without contact
2) Measurement under strong lighting
3) A compact mechanism that does not interfere with the surgical field
4) Intraoperative and immediate measurement
5) Following error within 0.5 mm at inclines of up to 45 degrees
6) A velocity of the micro laser in operation of 2–4 mm/sec

In this research, the following error from the target was set at less than 0.5 mm, which is half of the focal depth of the micro laser.

B. System Configuration and Measurement Method

Fig. 2 shows the system configuration of our automatic focusing system. In the system, position measurement was

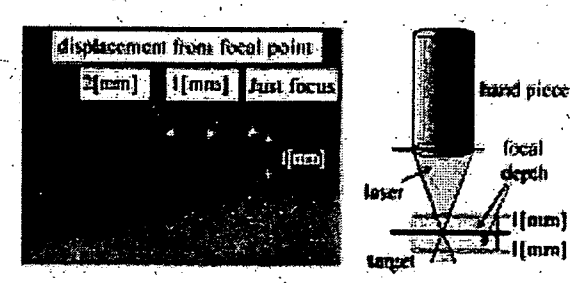

Fig. 1. Focal depth of the micro laser.

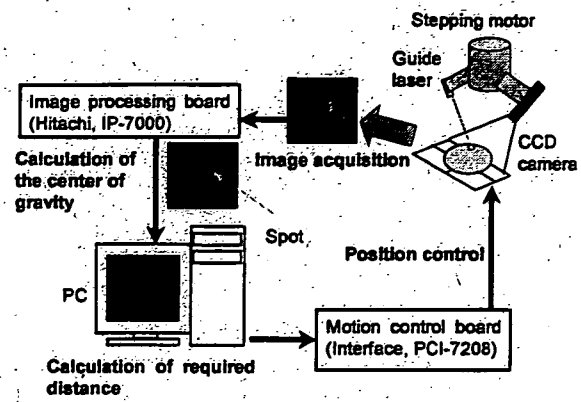

Fig. 2. Overview of the automatic focusing system. First, the system acquires an image using the CCD camera. The guide laser spot is extracted and the image processor calculates the coordinate of its center of gravity. The distance of the focal point from the target brain surface is calculated using a triangulation method. This error is sent to the motion controller and the stepping motor corrects the position.

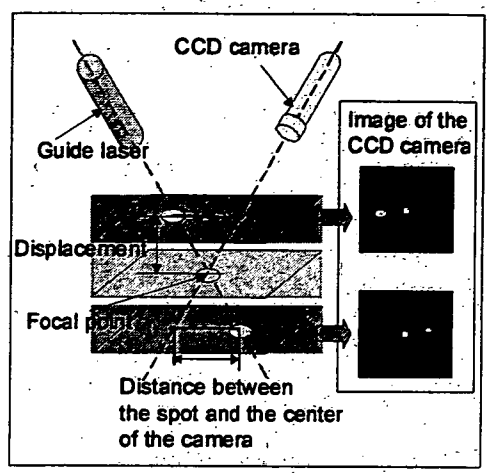

Fig. 3. Measurement principle.

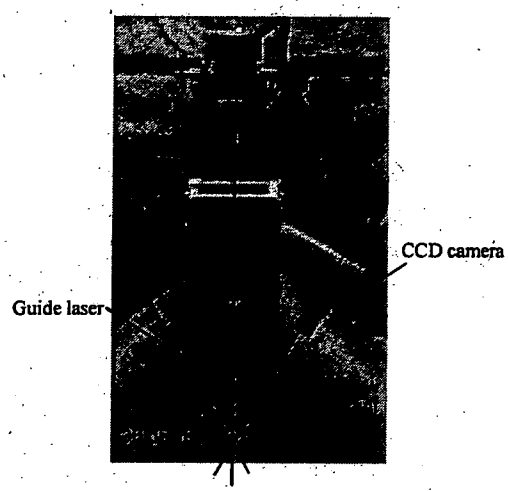

Fig. 4. Prototype of this system. The guide laser with wavelength of 532 nm and the CCD camera for measurement is set at the angle of 30 degrees

performed using a triangulation method, with a guide laser and a small CCD camera for measurement. The advantage of this method is that as light for treatment, with a wavelength of 2.8 μm, is not visible, the surgeon can identify the treated point by looking at the guide laser. In addition, as the mechanism is simple, it was easy to realize a compact device.

The guide laser and the CCD camera were fixed so that the axes of each component crossed at the focal point of the ablation laser (Fig. 3). If the focal point passes along the target surface, the spot of the guide laser is observed at the center of the screen of the CCD camera. The distance between the surface of the target and the focal point was calculated based on the displacement of the guide laser spot on the CCD image. Focusing was performed by continuously monitoring the displacement of the spot.

Fig. 4 shows a prototype of this system. The length of the device was 225 mm. The weight without the ablation laser module was 0.6 kg. A laser diode with a wavelength of 532 nm was used for the guide laser. Although a red laser diode is more practical, light penetration into biological tissue is stronger than with the green laser, and as this penetration causes positioning error, as described in the next chapter, we selected the green laser diode.

The operating frequency of the system was determined by the image acquisition cycle of 16.7 ms, the computing time for the image processing, and the positioning time of the stepping motor. The time for image processing was about 16 ms or more, and the time for positioning was often less than 50 ms. The drive of the motor was processed simultaneously with the image acquisition and processing. Therefore, the operating period of this system was approximately 50 ms.

The setting angle of the CCD camera and the guide laser was 30 degrees from the driving direction of the system. The resolution of the system, based on the resolution of the CCD camera, was 0.024 mm.

The electric shutter speed was normally set to 1/4000 s. The camera used in this research could increase the speed to 1/10000 s. The purpose of increasing the shutter speed is to cut noise from lighting and diffuse reflections. The image obtained was sent to the image processor, binarized by luminance level (eight bits), and spot extraction performed.

III. Image Processing Technique

The light radiated onto biomedical tissues is attenuated and penetrates the tissue according to its scattering and absorption features [5], [6]. These optical properties vary with the type of target, for example brain cortex, white

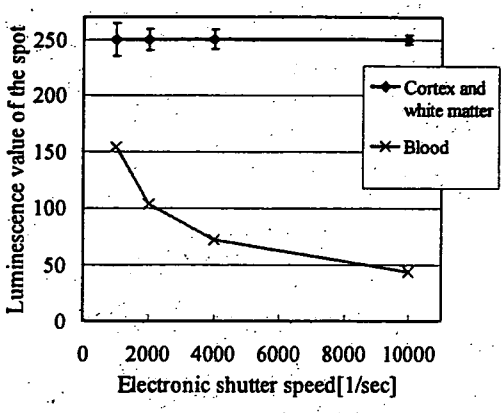

Fig. 5. Difference in the luminance value of the spot by the irrigated object.

matter, or blood. We examined the relationship between target tissues and spot extraction. From this pilot study, we developed an appropriate spot extraction method for biomedical tissues.

A. Spot Extraction Issues

Fig. 5 shows the differences in the luminance values of the spot according to the object irrigated. The horizontal axis is the electronic shutter speed of the CCD camera and the vertical axis is the luminance value of the spot. The tested objects were porcine cortex and white matter, and rat blood. Extraction of the spot was difficult in blood compared with brain parenchyma. To extract the spot successfully, it was necessary to lower the threshold in blood. On the other hand, if the threshold was too low, noise occurred, and extraction of the spot became impossible.

This system determines the coordinates of the spot by measuring its center of gravity. These coordinates contain error caused by penetration of the biomedical tissue. This is because the camera catches the light from the inside of the tissue. Fig. 6 shows the relationship between the error and the area of the extracted spot. The test was performed on a phantom of Intralipid-10% [6], [7]. Its scattering coefficient at the wavelength of 532 nm was 3 cm^{-1}, which is near the value of gliomas [5]. If the area of the spot was large, the error increased.

B. Threshold Control

If a luminance threshold is fixed to a high level, for a target such as blood it was impossible to extract the spot in some conditions. However, if the luminance threshold is low, the area of the spot becomes large, and then the error becomes larger. It is desirable to control the luminance threshold to an appropriate value, so that the area of an extracted spot is constantly small. We developed a threshold controlling method based on the relationship between the luminance threshold and the area of an extracted spot.

We used a single mode fiber for the green guide laser with a wavelength of 532 nm. Its light intensity distribution depends on the normal distribution. If a target has only

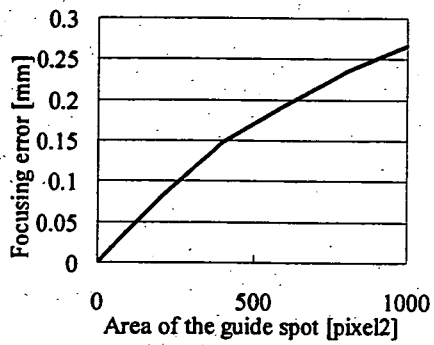

Fig. 6. Relationship between the error and the area of the extracted spot.

isotropic back scattering and no laser penetration efficiency, the relationship between light intensity and the distance from the center of a laser spot is (1).

$$I \approx \exp\left(-d^2/2\sigma^2\right)/\sqrt{2\pi}\,\sigma \tag{1}$$

where

I = light intensity,
d = distance from the center of a laser spot,
σ = standard deviation of the distribution.

Although the laser penetrates into brain tissues, the relationship between light intensity and the distance from the center of a laser spot is similar to (1). The relationship between the luminance threshold and the area of an extracted spot was derived from (1). The luminance threshold corresponds to light intensity and the area of an extracted spot corresponds to the square of the distance from the center of a laser spot (2).

$$Y = a\exp(-bA) + c \tag{2}$$

where

Y = luminance threshold,
A = area of spot,
a, b, c: constants—dependent on the target conditions.

Fig. 7 shows the relationship between the luminance threshold and the area of an extracted spot, and a curve approximated from (2) for white matter. The values of a, b, c differ according to the target tissue conditions. These three numbers were obtained with the luminance threshold Y, the area of an extracted spot A, and a histogram of luminance levels as follows:

1) A histogram of luminance levels was taken for a color image before binarization.
2) c is the asymptotic value of the luminance threshold. We determined it as the value 40% from the top of the histogram, where the area of the spot exponentially increased.

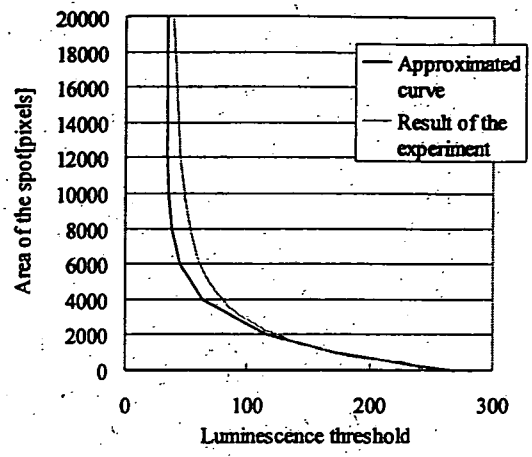

Fig. 7. Relation between the luminance threshold and the area of the extracted spot and an approximated curve in white matter.

3) At the peak value of the histogram, Y_{max}, the area of the spot $A = 0$. a was determined as follows: (3)

$$Y_{\max} - c = a\exp(-b \times 0) = a \tag{3}$$

4) Then b was determined from Y and A (4).

$$b = -\ln((Y-c)/a)/A \tag{4}$$

When focusing, the approximated function was calculated using the above method for every process. We could assume the appropriate value of the luminance threshold used in the next process by this approximated function. The method of controlling the luminance threshold was as follows. Before focusing, A_0 was set as the desired value of the area of the spot: sufficiently small to reduce the error due to penetration.

0) Focusing started.
1) The area of a spot, A_n, was obtained with the luminance threshold Y_n.
2) The approximate function for the relationship between Y_n and A_n was calculated (5).

$$Y_n = a_n \exp(-b_n A_n) + c_n \tag{5}$$

3) Y_{n+1} was computed as follows (6), and used for the next process.

$$Y_{n+1} = a_n \exp(-b_n A_0) + c_n \tag{6}$$

4) Return to 2).

As the device is moving at a speed of 2–4 mm/sec and the target tissue is being ablated while focusing, the condition of the target tissue is changing with time. Therefore, the assumed value of the threshold based on the current process is not perfectly adapted to the next process. However, the operating period of this system is 50 ms and the distance moved during this period is 0.1–0.2 mm, and thus the conditions of the target may not differ much in each consecutive process. Therefore, this method may be sufficient to allow stable extraction of the laser spot. In the following chapter, we compared this method with a method using a fixed threshold.

IV. Experiment

The experiments evaluating positioning accuracy, following error, and the threshold control methods are described in this chapter. These experiments were performed without ablation with the micro laser. Tests in combination with the micro laser will be performed in the future.

A. Experimental Evaluation of Positioning Accuracy

As an initial point, a focal point for the device was set on the horizontal target plane. The device was then moved vertically ± 0.4 mm from the focal point. Focusing was performed, and we measured the positioning error.

The average of the results was 0.04 mm, with a standard deviation of 0.05 mm, results fulfilling the desired specifications. The positioning accuracy of the stepping motor used in this system is 0.02 mm. The resolution based on the resolution of the CCD camera is 0.024 mm. These were considered as the main factors in the error.

B. Experimental Evaluation of the Following Error

The following error was measured for ascending and descending slopes. The angle of the slope was 45 degrees. Focusing was performed to the slope in a vertical direction. The device moved horizontally at a constant speed of 1, 2, 4, and 6 mm/sec. The distance moved was 10 mm.

The device followed the slope with constant delay at any traveling speed. There was no significant difference between ascending and descending slopes. The delay increased in proportion to the traveling speed (Fig. 8). These results fulfilled the desired specification of 0.5 mm.

C. In Vitro Threshold Control

We compared the method of dynamically changing the

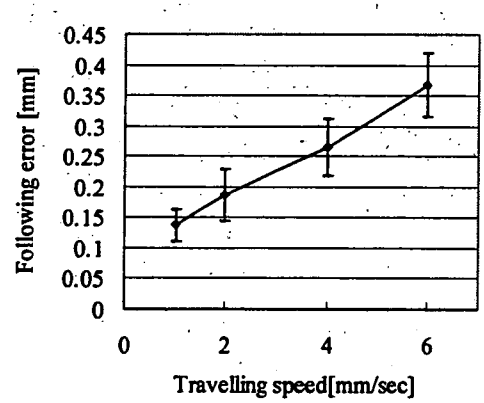

Fig. 8. Average of the following error with each traveling speed.

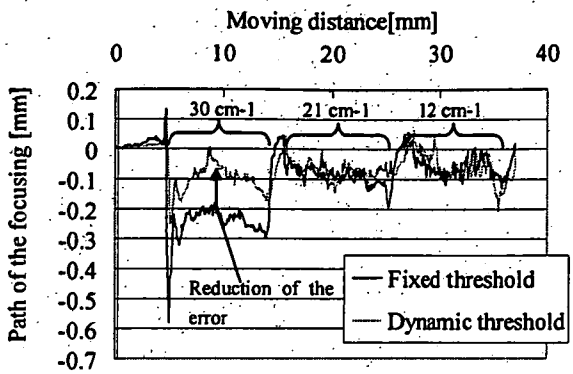

Fig. 9. Paths of the device *in vivo* experiment. The blue line is the path with the fixed threshold. The red line is the path with the dynamically changed threshold.

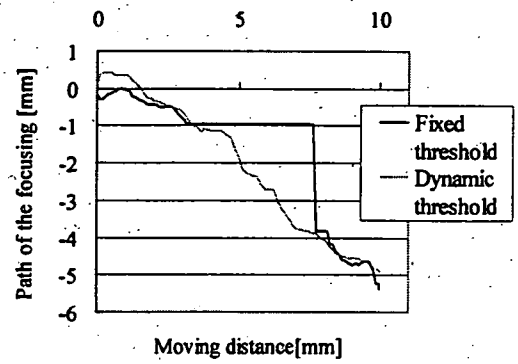

Fig. 10. Paths of the device *in vitro* experiment. The blue line is the path with the fixed threshold. The red line is the path with the dynamically changed threshold.

TABLE I
AVERAGE AND STANDARD DEVIATION OF THE AREA OF THE EXTRACTED SPOT.

		Method of the Threshold	
		Fixed	Dynamic
Area of the extracted spot [pixel]	Average	463	48
	Standard deviation	111	46

TABLE II
AVERAGE AND STANDARD DEVIATION OF THE AREA OF THE EXTRACTED SPOT AND THE SUCCESS RATE OF THE SPOT EXTRACTION.

		Method of the threshold	
		Fixed	Dynamic
Area of the extracted spot [pixel]	Average	101	78
	Standard deviation	102	62
Spot acquisition rate [%]		30	100

luminance threshold with a method using a fixed threshold. The device was consecutively moved on a phantom composed of Intralipid-10% [6], [7] with three different scattering coefficients, aligned in the order of 30, 21, and 12 cm^{-1} at the wavelength of 532 nm. The coefficient of 30 cm^{-1} is similar to that of white matter [5]. The width of each part was 10 mm and the interval between the parts was 1 mm. Focusing was performed using the two methods. The velocity of the device was 2 mm/sec horizontally. In the method of controlling the threshold, the desired value of the spot area A was set to 50 pixels. The luminance threshold was set to 100 in the fixed threshold method.

The paths of the device are shown in Fig. 9. The error was minimal on the 30 cm^{-1} part; reduced to 0.14 mm on average with the dynamically changing method. The area of the extracted spot was smaller and less variable with the dynamically changing method (Table I). As the spot was rather large and luminous on the 30 cm^{-1} part, this method worked most effectively.

D. In Vivo Threshold Control

Two methods for luminance thresholding were evaluated in *in vivo* experiments. The target was the surface of a porcine brain exposed by craniotomy under anesthesia. Focusing was performed while moving 10 mm horizontally at 2 mm/sec. In the method controlling the threshold, a desired value of the spot area A was set to 50 pixels. The luminance threshold was set to 100 in the fixed threshold method.

Fig. 10 shows the paths of the device. In the middle of the line, it was impossible to extract the guide spot using the fixed threshold method. Table II shows the data related to the extracted spots as the average and standard deviation of the area of the spots and the success rate of the extraction. Although the success rate of the fixed threshold method was only 30%, that of the controlling threshold method was 100%. Although the two lines in Fig. 10 indicate the same line on the porcine brain, they do not coincide. It is assumed that the reason for the difference was pulsation of the brain surface.

V. DISCUSSION AND CONCLUSIONS

We have developed a compact automatic-focusing system for micro laser instruments for neurosurgery. The wavelength of this laser is 2.8 μm and the laser is used for precise ablation of brain tumors. In this system, position

measurement was performed using a triangulation method with a guide laser and a small CCD camera. A surgeon can identify the treated point by looking at the guide laser. As the mechanism is rather simple, it was easy to realize a compact device.

The light radiated onto biomedical tissues is attenuated and penetrates the tissue according to its scattering and absorption features. According to the condition of the target, the appropriate value for each measurement parameter was different. For example, it was necessary to appropriately control the luminance threshold in the image processing, and we developed a new technique for controlling the threshold.

The positioning accuracy and the following error of this system were evaluated. The results fulfilled the desired specifications.

The methods of controlling the threshold and using a fixed threshold were compared. In *in vitro* experiments, the error when controlling the threshold was less than when using the fixed threshold. In *in vivo* experiments, the error was also reduced, and the success rate of the spot extraction improved greatly. The threshold controlling method effectively worked for biomedical tissue.

The evaluations performed in this paper did not consider the pulsation of the brain surface. As it is assumed that the human brain has a certain amount of the pulsation, it is necessary to evaluate the effects of pulsation on following error.

In the future, we will perform tests in combination with the ablation laser to achieve a precise system for operation upon brain tumors.

ACKNOWLEDGMENT

We wish to thank many people and groups who have contributed to this effort. One of them deserving special mention is Yasuo Oda of chief engineer of Biomedical Precision Engineering Laboratory, the University of Tokyo. The research funds was based in part on Grant-in-Aid for Scientific Research of JSPS (# 15700349) and Terumo Lifescience Foundation.

REFERENCES

[1] T. Maruyama, et al, "Intraoperative detection of malignant gliomas using 5-Aminolevulinic acid induced protoporphyrin fluorescence, openMRI and real-time navigation system," Computer Assisted Radiology and Surgery, vol. 15, pp. 270-275, 2001.

[2] K. Shimizu, et al, "Application of blue semiconductor laser to measurement of 5-ALA induced fluorescence for intraoperative detection of brain tumor," Proceedings of 6th Japan-France Congress on Mechatronics and 4th Asia-Europe Congress on Mechatronics, 2003, pp. 135-140.

[3] S. Omori, Y. Muragaki, I. Sakuma, and H. Iseki, "Robotic laser surgery with λ = 2.8um microlaser in neurosurgery," Journal of Robotics and Mechatronics, vol. 16, no. 2, pp. 122-128, 2004.

[4] S. Omori, R. Nakamura, Y. Muragaki, H. Iseki, K. Takakura, Improvement study of computer controlled mid-infrared laser system for neuro-surgery, Proceedings of 13th conference of Japan Society of Computer Aided Surgery (JSCAS), pp. 37-38, 2004

[5] Sterenborg HJ, et al, "The spectral dependence of the optical properties of the human brain," Lasers Med Sci, vol. 4, pp. 221-227, 1989.

[6] "Optical properties spectra," http://omlc.bme.ogi.edu/spectra/.

[7] J. van Staveren, J. M. Moes, J. van Marle, A. Prahl, J. C. van Germert, "Light scattering in Intralipid-10% in the wavelength range of 400-1100 nm," Appl Opt, vol. 30, pp. 4507-4514, 1991.

Improvement of Compact Forceps Manipulator using Friction Wheel Mechanism

Takashi Suzuki, Youichi Katayama, Etsuko Kobayashi and Ichiro Sakuma

Graduate School of Frontier Sciences, The University of Tokyo

7-3-1, Hongo, Bunkyo-ku, Tokyo, 113-8656, Japan
t-suzuki@miki.pe.u-tokyo.ac.jp

Abstract: This paper reports improvement of compact forceps manipulator designed for assisting laparoscopic surgery, and reports mechanical performance evaluation and *in vitro* experiment to simulate the clinical use. The manipulator consists of two parts; friction wheel mechanism (FWM) which rotates and translates the forceps (62×52×150 [mm^3], 0.6 [kg]), and gimbals mechanism which provides the pivoting motion of forceps around the incision hole on the abdomen (135×165×300 [mm^3], 1.1 [kg]). We adopted new friction wheel mechanism instead of former prototype. The results of evaluation showed that the new FWM contributed to the quick motion. In spite of trade-off between speed and force, the required force was satisfied. Positioning accuracy of FWM was less than 0.2 [mm] in translation and 0.8 [deg] in rotation. *In vitro* experiment revealed that the manipulator provided stable motion even if the liquid material such as blood attached onto the forceps, which would be a cause of slip between friction wheel and the surface of forceps. The new manipulator was promising and useful in laparoscopic surgery.

Introduction

Laparoscopic surgery is a less traumatic therapy and widely performed as one of minimal invasive surgeries. It requires great skill to surgeon because surgical instruments with long-handle decrease the tactile sensation and the dexterity of the hand. Responding to this problem, surgery-assisting robotic systems with maneuverable robotic arms and laparoscope manipulator are developed, and some of them are commercially available. While several positive feasibility studies are reported, disadvantages to those systems are also pointed out, and one of them is the size [1]. Today's crowded-operating room might not have enough space to install robotic arms. Large-sized robotic arms cover operating space above the patient, and also have potential danger of collision with medical staffs or patient. Miniaturized surgical robotic systems are, therefore, required [2].

We have developed a compact forceps manipulator using "friction wheel mechanism" (FWM) [3] and gimbals mechanism. In the former study, prototype was fabricated and feasibility study was conducted as a forceps manipulator [4]. In later study, it was found that the rotational speed of ultrasonic motor varied depending on the load, so that the unstable motion of the motor led to unstable motion of the forceps [5]. Responding to this problem, we reported that the modification of machining accuracy and the semi-closed feedback control increased the performance of the manipulator [6]. In this study, we adopted new friction wheel mechanisms instead of former prototype to realize efficient quick motion. This paper reports mechanical configuration and performance evaluation. We lastly discuss the improvement of the manipulator comparing with the former prototype and the future perspective.

Materials and Methods

We set the following requirements for the manipulator. (1) Miniaturization to install at least three sets in the operating field, corresponding to both hands of surgeon and one hand of assistant. (2) Mounting on the surgical table for easy setup and easy detachment. (3) Four degrees of freedom (DOF); pivoting motion around incision hole, and rotation and translation of forceps. (4) Enough power. It can bear 4[N] of weight considering the third weight of liver (approximately 0.4 [kg]).

To satisfy the abovementioned requirements, we adopted following two mechanisms; "Friction wheel mechanism" (FWM) provides the rotation around the forceps shaft, and provides translation along the shaft (circled number 1 and 2 in Figure 1). Gimbals mechanism is used to provide pivoting motion (3 and 4 in Figure 1) [4]. We mount this manipulator near the incision hole. This is because mechanisms and actuators should be mounted near the operating field so that they require less torque or force [2].

We used "friction wheel" that consisted of three titled idle rollers and outer case (Figure 2(a)) [3, 7]. When outer case rotates, rollers passively travel spirally on the surface of shaft (Figure 2(b)). We have two kinds of FWM with opposite tilting angle. They are like right-handed screw and left-handed one. Each FWM makes spiral motion in each direction respectively. We combine the two motions to realize rotation and translation (Figure 2(c)). For the rotation, we rotate both friction wheels in the same direction (Figure 3). In this case, rollers do not rotate, and do not make spiral motion. Thus, the shaft held statically by rollers rotates at the same speed as the FWM. As for translation, we rotate each FWM in the opposite direction (Figure 3). Each rotational motion is cancelled mutually, and only translation remains, thus longitudinal translation is realized. We adopted a hollow-shaft ultrasonic motor with rotary encoder (custom order, Fukoku, Japan) to drive FWM.

The tilting angle of FWM affects the speed and force of feeding motion like the pitch of feed screw. As the same that a screw with wider pitch provides higher feeding speed and lower power, we can realize higher driving speed by changing the tilting angle of FWM. In the former study [6], the mechanical evaluation of former prototype with tilting angle of 30 [deg] showed the enough force. We, therefore, decided to change the angle to accelerate the feeding speed. The tilting angle of new FWM was set at 45 [deg] in this study. Speed and force of translation are direct proportional to sine/cosine function of tilting angle, thus we estimated that the speed would increase by a factor of 1.4 (= sin 45 [deg] / sin 30 [deg]) and force would decrease by a factor of 0.82 (= cos 45 [deg] / cos 30 [deg]).

We realized feedback-loop control using rotary encoders to match the speed of both motors. Driving software was also developed to cancel the slight difference between two spiral motions caused by machining error.

The new prototype is shown in Figure 4. Weight is 1.7 [kg]. FWM was 62×52×150[mm^3], 0.6[kg], and gimbals mechanism was 135×165×300[mm^3], 1.1[kg]. Appearance is the same as the former prototype [6].

Results

Mechanical performance evaluation was conducted. We firstly measured the torque and force using 6-DOF strain gauge sensor (MINI sensor 8/40, BL AutoTech, Japan), and measured the speed using digital microscope (VH-7000, KEYENCE, Japan). Results are shown in Table 1. We set the diameter of forceps as 5 [mm], thus, the required rotational torque was 1.0×10^{-2} [Nm] and required translation force was 4 [N]. Measured results satisfied the requirements.

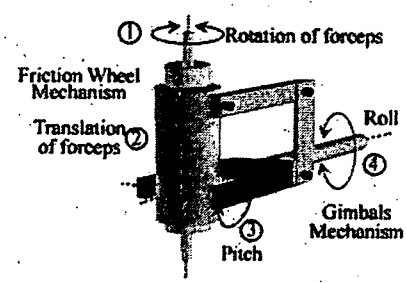

Figure 1: System configuration. Manipulator consists of friction wheel mechanism and gimbals mechanism.

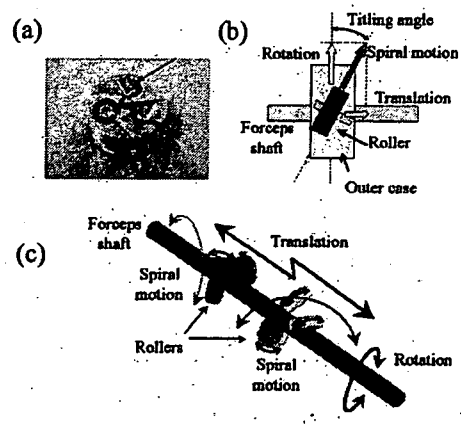

Figure 2: Friction wheel mechanism (a) friction wheel (b) titled roller provides spiral motion (c) rotation and translation are realized with two spiral motions.

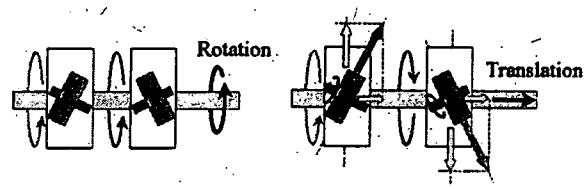

Figure 3: Mechanism of rotation and translation.

We also estimated that the positioning accuracy of translation would decrease as the tilting angle of FWM changed. We measured the positioning accuracy of the manipulator without load. Results are shown in Figure 5. Positioning accuracy was less than 0.2 [mm] in translation and 0.8 [deg] in rotation. The result did not show the significant performance degradation comparing with [6].

Our manipulator realizes translation and rotation using two different spiral motions. If they are not symmetrical perfectly, error motion occurs, so that the motion of forceps gets unstable. Responding to this problem, we implemented a driving software to cancel the unstable motion. We measured the errors, that is, translation error was measured when rotation command of 10 revolutions was input, and rotational error was measured when translation command of 50 [mm] was input. Results are shown in Table 2. Comparing the accuracy with that of old prototype, significant decrease of positioning accuracy was not observed depending on the tilting angle of FWM.

Lastly, we investigated the positioning error caused by slip between FWM and the surface of forceps. In a clinical situation, if liquid matter such as blood attaches on the forceps, the coefficient of static friction decreases, so that slip would easily occur. The position of the forceps is calculated from the incremental pulse signal, thus, once slip occurs and the position is lost, the manipulator will malfunction. To prevent the problem, we simulated the clinical use and conducted *in vitro* experiment using heparinized blood of rat. Forceps shaft coated with blood was set vertically, and load was mounted at the lower end of the shaft. We measured the load when the shaft started to slip. Results are shown in Table 3. Comparing with the result of the former prototype, the maximum withstanding load decreased to 15[N]. It was, however, found that the required specification of 4 [N] was satisfied in spite of liquid matter that encouraged the slip.

Table 1: Results of mechanical performance of new prototype and comparison with former prototype

	New prototype	Former one
Rotation speed [rpm]	41.8 ± 0.4	41.8 ± 0.6
Rotation torque [Nm]	$6.1 \pm 0.8 \times 10^{-2}$	$6.3 \pm 0.9 \times 10^{-2}$
Trans. speed [mm/s]	11.2 ± 0.1	6.5 ± 0.1
Translation force [N]	31.6 ± 1.8	61.0 ± 0.7

Table 2: Comparison of positioning errors caused by the unstable motion of motor.

	New prototype	Former one
Rotational error in translation	1.1 ± 0.8 [deg]	1.1 ± 1.1 [deg]
Translation error in rotation	0.0 ± 0.0 [mm]	0.0 ± 0.0 [mm]

Table 3: Maximum load without slip.

	New prototype	Former one
Without blood	20 [N]	20 [N]
With blood	15 [N]	20 [N]

Discussion

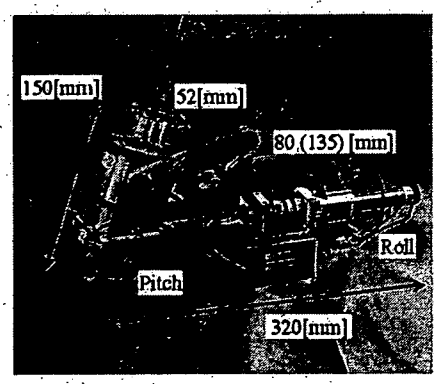

Figure 4: New prototype.

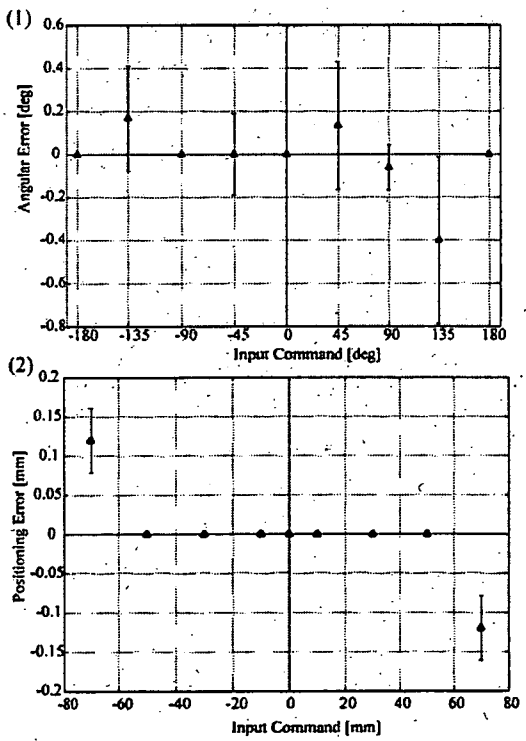

Figure 5: Results of evaluation tests. (a) angular error in rotation. (b) positioning error in translation

In this study, we conducted installation of new FWM with tilting angle of 45 [deg], and evaluated its performance and feasibility in clinical situation. The mechanical performance evaluation showed that the new FWM increased the speed of translation. This will contribute to quick response. The translation force decreased because of the trade off between speed and force, however, the required force was satisfied with enough margin. Contrary to our expectations, position accuracy of rotation and translation did not decrease. As the results of *in vitro* experiments, the maximum withstanding load decreased comparing with the former prototype. The required force of 4 [N] was satisfied adequately. Because we still have enough torque margin, we will optimize the tilting angle of the FWM to realize more efficient driving. The forceps manipulator using FWM consequently showed the improvement in the speed of translation and no degradation of other mechanical performances.

We have two plans as future works. Firstly, we are going to integrate a position sensor to measure the position of the forceps directly. Secondly, we will redesign our manipulator to realize sterile-compatible one. In our system, as mentioned above, the position and speed of the forceps are calculated from the rotation number and speed of the incremental rotary encoder mounted on the ultrasonic motor. It is the drawback of this system, that is, the position obtained from the sensor is relative position and not absolute position. Once the position of the forceps is lost because of errors such as slip, we have to initialize the position sensor, or the manipulator will malfunction. External position sensing device is required. Among the commercialized sensing devices, optical tracking system (for example, Polaris®, Northern Digital Inc., Canada) or magnetic tracking system (for example, microBIRD™, Ascension Technology Corp., USA) can be candidates for the purpose, although they have weaknesses to disturbance. As for the second work, we will redesign our manipulator to implement a detachable transmission mechanism, such as an idle gear unit. In the case of malfunction, this mechanism can work mechanical shutoff system by detaching the transmission gear. This kind of mechanical safety device should be implemented adding to electric sensors and software emergency routines as redundant safety. The transmission mechanism, at the same time, can work as coupling device between sterilized and non-sterilized parts [8].

Conclusions

We installed new FWM into the forceps manipulator in this study. It provided quicker translation than former prototype and satisfied the required specifications. We are convinced of the usability of the manipulator in the field of computer aided surgery.

Acknowledgement

This work is partially supported by "Research for the Future Program (JSPS-RFTF 99I00904)" funded by Japan Society for the Promotion of Science, Electro-Mechanic Technology Advancing Foundation, "Research and Development of the Compact Surgical Robot System for Future Medical Care" funded by New Energy and Industrial Technology Development Organization, and "Research on medical devices for analyzing, supporting and substituting the function of human body" funded by Ministry of Health, Labour and Welfare.

References

[1] A.R. Lanfranco, et al. Robotic surgery: A current perspective. Annals of Surgery, 239(1): 14–21, 2004.

[2] Y.Kobayashi, et al. Small occupancy robotic mechanisms for endoscopic surgery. In Proc. MICCAI 2002, Part 1, pages 75–82, 2002.

[3] M.Vollenweider, et al. Surgery simulator with force feedback. In Proc. 4th International conference on motion and vibration control (MOVIC98), 1998.

[4] T.Suzuki, et al. A new compact robot for manipulation forceps using friction wheel and gimbals mechanism. In Proc. CARS2002, pages 314–319, 2002.

[5] Y.Katayama, T.Suzuki, et al.; New compact robot for manipulating forceps using friction wheel and gimbals mechanism, In Proc. of Semestrial Conference of Japan Society for Precision Engineering, pp. 742, 2004.

[6] T.Suzuki, et al., Compact forceps manipulator for laparoscopic surgery, IEEE/RSJ international conference on intelligent robots and systems, submitted, 2005.

[7] http://www.zero-max.com/products/rohlix/rohlixmain.asp

[8] J.L.Hefti, et al. Robotic three-dimensional positioning of a stimulation electrode in the brain. Journal of Computer Aided Surgery, 3(1): 1–10, 1998.

Design and Evaluation of a Master-Slave System with Portability and Flexibility of Setting

E.Aoki*, T.Suzuki*, E.Kobayashi*, M.Hashizume** and I.Sakuma*

* Graduate School of Frontier Sciences, The University of Tokyo
** Department of Disaster and Emergency Medicine, Graduate School of Medical Sciences, Kyushu University

{aoki,t-suzuki,etsuko,isakuma}@miki.pe.u-tokyo.ac.jp
{mhashi}@dem.med.kyushu-u.ac.jp

Abstract: This paper describes a master slave system to have the following functions. 1) Portable master-slave system that can be divided into each surgical device easily. 2) Setting method can be changeable according to the operation environment. To realize above functions, we use a three dimensional optical tracking sensor to regard each surgical device attached portable optical marker as a module which has 3D position information. Using this method, enabled master-slave to be easily dedicated to each surgical device, making it more compact and easier to move, with advantages for military use. In an evaluation experiments, the overall positioning errors less than 2 mm showed the feasibility of our master-slave system using optical tracking system for a laparoscopic surgery.

Introduction

Master–slave systems have been widely studied and have been shown to enhance the dexterity and abilities of surgeons[1][2][3]. Da-Vinchi® system has been already available commercially and been used in a clinical application[4]. These systems consist of a master arm system (master) and a slave manipulator system (slave). In the master system, a surgeon sits in front of a monitor showing a laparoscopic view and controls the master manipulators. The slave consists of an endoscope and various manipulators, depending on the operation. Thus, master-slave system is a large-scale system and usually all-in-one systems that can not be divided into each surgical device easily. As one example of application, master-slave systems are expected to realize telesurgery, for example it is famous that da Vinchi® was developed for military use[5]. However, most master-save systems are not satisfactory for actual use of these applications because they have difficulty in carrying. Assuming master-slave systems are used in clinical application, it is required to appropriate setting depending on each surgical procedure.

Therefore, we developed portable master-slave system, which can be divided into each surgical device easily for portability and can be set freely accordint to surgical situation.

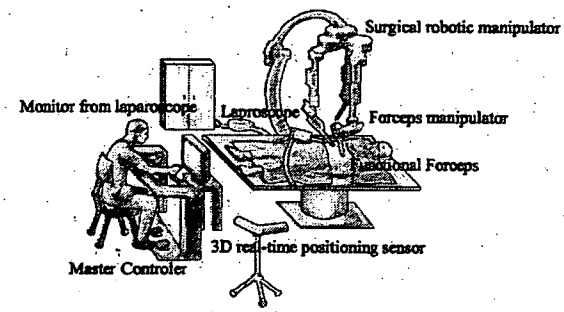

Figure.1 Concept figure of master-slave system

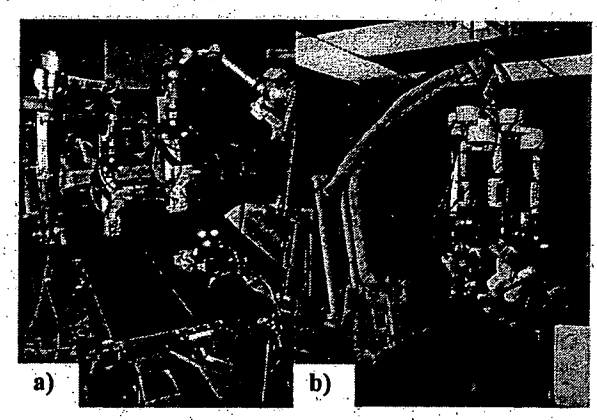

Figure.2 Two kinds of setting using surgical robotic manipulator, a)"bedside" arm and b) "suspending" arm

Materials and Methods

A) Realizing of Portability

It is important to deal with the integrated position information to realize master-slave system and keep the whole system consistent. However, our master-slave system is consists of stand-alone surgical devices that are independent and can be used individually.

Our master-slave system consists of stand-alone surgical devices that were developed independently and can be used individually for portability. It is sure that using this method makes it more compact and easier to move, with advantages for military use, but, we have to connect independent each surgical device for integrating coordinate.

Therefore, we thought to use a external positioning sensor to measure the setting position of surgical devices.

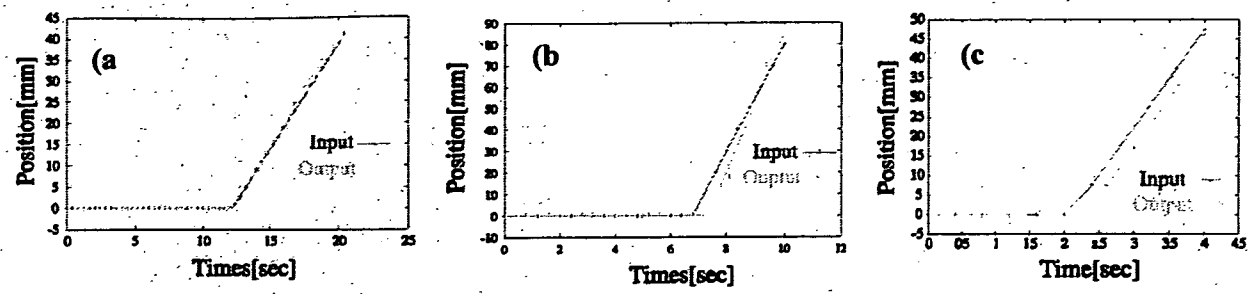

Figure 3. Experimental result of Positioning accuracy: a) in X axis, b) in Y axis, c) in Z axis

Table.1 Positioning accuracy of forceps manipulator

	Mean error[mm] (n=3)
X axis	0.28±0.74
Y axis	1.41±4.11
Z axis	1.96±2.60

As a positioning sensor, we adopted a three dimensional optical tracking sensor(Polaris®, Northern Digital Inc. Canada). Optical markers were mounted at the end of the device and were measured from the sensing unit that emitted the infrared light and received reflected light. The performance of sampling frequency is 30[Hz] and RMS(Root Mean Square) of this device is about 0.35[mm]. No angle sensors such as rotary encoder or potentiometer were mounted. Although it is sure that mechanical method is superior to optical method from the aspect of accuracy, optical method has following advantages.

1) Surgical devices with optical tracking markers can be regarded as modules having the position information.

2) Miniaturization of the surgical devices can be achieved because the method does not require electric wiring.

Above methods enabled our master-slave system to be divided into various surgical devices easily and to integrate each surgical device independently. The concept figure of our developed master-slave system was shown as Fig.1.

B) Realizing of flexibile setting

]There are two kinds of surgical robotic manipulators in the point of mechanical setting up; one is "suspending" arm (ex. da Vinci(R)), and the other is "bedside" arm (ex. ZEUS(R)). Bedside arm has advantages in its small size and easier to move. However, it is clear that setting-up position is limited to the rail attached to the side of surgical table so that the setting-up procedure is complicated to avoid the collision between arms. On the other hand, suspending arm has advantage that flexible and intuitive positioning of manipulator is possible in the setting-up procedure. However, it is large size and difficult to move. Thus each surgical robotic manipulator has quite different character and it is desirable to use both "suspending" arm and "bedside" arm as the situation demands. For example, if we assume for military use, it should be "bedside" arm for easier to move. And if we only assume in clinical use, it should be "suspending" arm for easier to setting.

Since our master-slave system utilize optical tracking sensor and surgical devices with optical tracking markers can be regarded as modules having the position information, each surgical device is independent of surgical robotic manipulators. Therefore we can select appropriate setting method according to various requirements in the operation environments (Fig.2).

EXPERIMENTS & RESULTS

Since the system utilizes optical tracking system, surgical devices can be freely set in the operation environment. On the other hand, optical tracking sensor has larger measurement error comparing with electric encoder. Therefore, we confirmed our master-slave system has accuracy enough to surgical operation.

As a method of evaluation, we attached an optical tracking marker to the tip and the base of slave manipulator and measured the position of its marker by using the optical tracking sensor(Polaris®, Northern Digital Inc. ,Canada). The order on coordinate of endoscopic view was sent from virtual master to slave manipulator by means of TCP/IP (communication-rate was 10[Hz]) and the measurement frequency was 2.5[Hz].

The experimental results was shown as Fig.3 and the average and standard deviation at each axis was shown as Table.1.

DISCUSSION and CONCLUSION

In evaluation experiments, Table.1 shows that small positioning error was included, however, output almost follow input lead. The cause of positioning error was thought as follows:

1. Attached position of optical tracking marker.
2. Affection of mechanical vibration caused by the stiffness of suspending arm which holds slave manipulators.
3. Measurement error of optical tracking sensor.

The measurement error by using optical tracing sensor is commonly known as 0.3-0.4[mm]. This main error is vibration and attached position of optical tracking

marker [6]. One of the limitations of the optical marker based positioning system might be its accuracy. However, the overall positioning errors less than 2 mm showed the feasibility of our master-slave system using optical tracking system for a laparoscopic surgery.

We developed a master-slave system with portability and flexibility of setting. Our master-slave system could be easily dedicated to each surgical device, making it more compact and easier to move, with advantages for military use.

Acknowledgment

This study was partly supported by Research for the Future Program JSPS-RFTF 99I00904,Research and Development of the Compact Surgical Robot System for Future Medical Care, and Research on medical devices for analyzing, supporting and substituting the function of human body funded by Ministry of Health, Labour and Welfare.

REFERENCES

[1] K.Ikuta et al. Hyper-finger for Remote Minimally Invasive Surgery in Deep Area, Medical Image Computing and Computer-Assisted Intervention(MICCAI), pp173-181, 2002
[2] M.Mitsuishi et al. Development of a Remote Minimally – Invasive Surgical System with Operational Environment Transmission Capability, Proc. IEEE/ICRA2003, pp.2663-2670, 2003
[3] Y.Kobayashi et al. Small Occupancy Robotic Mechanisms for Endoscopic Surgery, Medical Image Computing and Computer-Assisted Intervention (MICCAI), pp75-82, 2002
[4] http://www.intuitivesurgical.com
[5] R.Khadem et al. Comparative Tracking Error Analysis of Five Different Optical Tracking System, Computer Aided Surgery, pp 98-107, 2000
[6] A.R. Lanfranco, et al. Robotic Surgery: A Current Perspective. Annals of Surgery, 239(1): 14–21, 2004